Numerical Methods in Civil Engineering

Journal Homepage: https://nmce.kntu.ac.ir/

Numerical Modeling of Roof Force in Concrete Liquid Storage Tanks

Pouya Soltani*, Hassan Mirzabozorg**

ARTICLE INFO

RESEARCH PAPER

Article history:
Received:
June 2024
Revised:
August 2024
Accepted:
September 2024

Keywords:
Sloshing, FE-SPH Coupling, Box-Behnken, Concrete Storage Tank, Fluid-Structure Interaction.

Abstract:

Liquid storage tanks are crucial in various applications, such as industrial processes and water supply systems. It's important to understand how these tanks behave during seismic events to ensure their structural safety. The freeboard is the space between the maximum liquid level and the tank's top edge. When the liquid sloshing height exceeds the designed freeboard, waves can impact the tank roof, potentially causing damage. This study examines the force applied to the roof of tanks when the freeboard is insufficient. The study used the Box-Behnken method for experimental design to conduct the analyses. Tanks were modelled using the finite element method combined with smooth particle hydrodynamics. The interaction of the stored fluid with the roof of the tank was assessed using the penalty technique and the soft constraint algorithm. The analysis showed that the combination of two parameters, the tank length and seismic stimulation, had the most significant impact. However, the fluid height was deemed a non-influential parameter when there was insufficient freeboard. Additionally, the results showed that the intensity acceleration spectrum accurately reflects the impact of frequency content on roofed tanks.

1. Introduction

Fluid-structure interaction (FSI) is a crucial concept in engineering, with applications spanning from aerospace to civil engineering and even biomedical fields. The complexity arises from the simultaneous need to solve the governing equations for both fluid flow and structural response, which are inherently coupled and dynamically influence each other. Reliable FSI analysis is critical for the design and safety of structures that interact with fluids, such as aircraft wings, turbine blades, blood vessels, and dams. Robust numerical methods are essential for predicting the complex phenomena occurring during these interactions, including turbulence, cavitation, and aeroelasticity.

Traditional mesh-based methods like the Finite Element Method (FEM), Finite Volume Method (FVM), and Finite Difference Method (FDM) have been extensively used due to their well-established theoretical foundations and wide applicability. These methods discretize the computational domain into a mesh to solve the equations of motion for both fluids and structures.

However, they often struggle with mesh distortion in cases of large deformations or complex geometries, leading to inaccuracies or numerical instability. To overcome these limitations, several innovative techniques have been developed:

- Level Set method: This method represents the interface between fluids and structures using a continuous function defined over the computational domain. It is particularly adept at capturing evolving interfaces without the need for explicit interface tracking or mesh reconfiguration.
- Volume of Fluid (VOF) method: VOF is effective for tracking and locating free surface flows by filling the volume fraction of each computational cell with fluid or gas, allowing for a clear distinction between different phases.
- Lattice Boltzmann method (LBM): LBM simulates fluid flow by tracking the evolution of particle distribution functions on a lattice grid. It is well-suited for complex boundary conditions and can easily handle large deformations and moving boundaries.

These advanced methods enhance FSI simulations by providing greater flexibility and accuracy in capturing interaction effects. They are particularly useful in scenarios

** Graduate Student in Structural Engineering, Civil Engineering Department, K. N. Toosi University of Technology, Tehran, Iran.*
***Corresponding Author: Associate Professor, Civil Engineering Department, K. N. Toosi University of Technology, Tehran, Iran. Email: mirzabozorg@kntu.ac.ir*

https://doi.org/10.61186/NMCE.2406.1065

where traditional methods fall short, such as in simulations involving fluid mixing, multiphase flows, or highly dynamic interfaces. In this context, the FE-SPH coupling method emerges as a powerful solution. By coupling the FEM with SPH, this approach bridges the gap between fluid and structural domains. Notably, it allows for segment-based interface treatment, overcoming particle deficiency near contact surfaces. Furthermore, due to its meshless nature, the SPH method provides more accurate representation of large fluid particle displacements.

Fluid storage tanks are a critical component susceptible to earthquake damage. Seismic forces generated during an earthquake can exert significant dynamic loads on the tank's roof and walls, leading to deformation, buckling, or collapse. Multiple studies have explored the damage to tank roofs during earthquakes, providing valuable insights into the seismic vulnerability of these structures. Malhotra (2005-2006) [1, 2] developed a formula to calculate the height of insufficient free surface using engineering simplification methods, considering only the hydrostatic pressure in the contact area between the tank roof and the liquid. Yoshida et al. (2010) [3] investigated the structural integrity of single-deck floating roofs in cylindrical storage tanks during the 2003 Tokachi-Oki earthquake utilizing axisymmetric finite element analysis. Golzar et al. (2012) [4] discussed the problem of seismic sloshing in floating roof liquid storage tanks. They used the extended Hamiltonian variational principle to derive the equations governing the sloshing response. They concluded that the dimensionless sloshing heights for the roofed tanks are solely dependent on their first natural period. Livaoglu et al. (2012) [5] conducted a study on the damage to liquid storage tanks' roofs during the 2010 Canterbury earthquake in New Zealand. The research found that numerous tanks experienced deformation and roof buckling, leading to liquid leakage. The study also showed that tanks with rigid roofs were more susceptible to damage compared to those with flexible roofs. Godarzi (2015) [6] discussed the problem of seismic sloshing in double-deck floating roof (DDFR) liquid storage tanks. Fluid-structure interaction as well as the specific shape of a DDFR tank was considered. The conclusion is that for the seismic design of a DDFR, it is important to consider not only the overall movement of the DDFR but also the local effects of the hydrodynamic pressure of the liquid on the bottom plate. Hosseini et al. (2017) [7] addressed the issue of damaging seismic sloshing in floating-roof oil storage tanks. They used a Suspended Annular Baffle (SAB), hanging from the floating-roof, to reduce the maximum sloshing height and suggested that SAB reduces the maximum seismic sloshing height by an average of 80% and 40% for harmonic and seismic excitations, respectively. Nouraeidanesh (2018) [8] introduced a novel tank roof design aimed at reducing the high impact forces resulting from sloshing, conducting experimental studies using shaking table tests on a partially filled tank subjected to harmonic and different earthquake excitations. The study concludes that the suggested roof design can effectively decrease sloshing loads by an average of 50% for the tested dimensions. Soltani et al. (2024) [9] measured the sloshing height during seismic excitation utilizing the FE-SPH method. The authors also used the Box-Behnken DOE method to evaluate the crucial parameter in sloshing height and demonstrated that the liquid height has the most contribution.

In this study, the Box-Behnken design of experiment is utilized. The Box-Behnken design (BBD) is a blend of a factorial design, which examines the effects of factors, and a central composite design, which explores the curvature of the response surface. This design is frequently employed to create an efficient experimental design for systems with multiple factors. It involves strategically selecting a subset of the possible combinations of factor levels to form a design matrix for the experiments. The matrix includes rows for each experiment and columns for each factor, squared term, and interaction term. The response surface model developed from this design is a second-order polynomial equation that links the response to the factors and their interactions. To assess the error and curvature of the response surface, experiments are replicated at the central point. In a three-factor Box-Behnken design, each factor represents a unique parameter that could impact the results. These factors vary along one dimension, with corner points representing extreme conditions (+1 or -1 for each factor), and centre points indicating the true centre of the region. The influencing factors are divided into three levels: low (-1), moderate (0), and high (+1). Figure 1 illustrates the central cube in the three-factor Box-Behnken design [10]. In this study, factor A represents seismic characteristics, factor B illustrates the tank length, and factor C represents the ratio of liquid height to tank length.

The primary objective of this study is to investigate how the sloshing phenomenon affects the dynamic responses of liquid storage tanks. We are specifically computing the force exerted on the tanks' roofs under varying earthquake conditions caused by insufficient free-board height. To achieve this, we are employing design of experiment methods to assess the effects of factors such as fluid height, tank length, and specific earthquake record characteristics like the ratio of maximum ground acceleration to maximum ground velocity (PGA/PGV) and the intensity acceleration spectrum (ASI). This study will also conduct an analysis of the individual effects of geometric parameters and earthquake record parameters to determine the most influential factor on tank response. Furthermore, mathematical formulations have been developed in order to accurately estimate the roof force in liquid storage tanks.

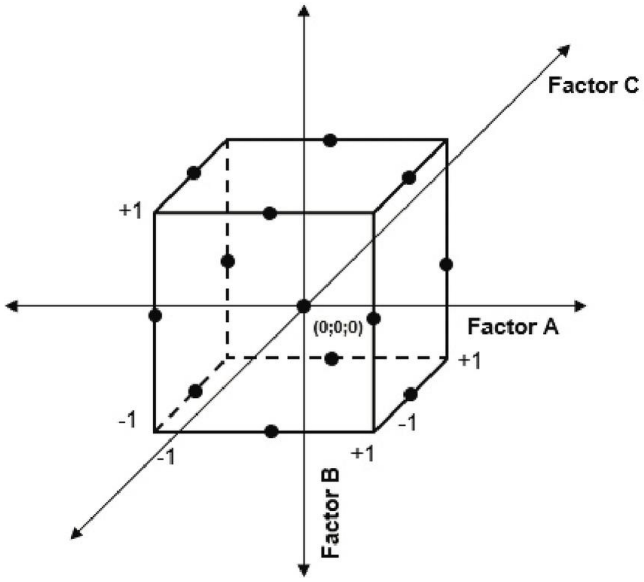

Fig. 1: The central cube in the three-factor Box-Behnken design [11].

2. Methodology

Lagrangian methods demonstrate more accurate performance than the SPH method, yet when confronted with large deformations, the SPH method proves to be more accurate. Therefore, the combination of finite element methods and smooth particle hydrodynamics enhances the accuracy of results for fluid-structure interaction problems. In this study, the same methodology, material properties, and earthquake records as [9] were utilized. Nevertheless, for the coupling method, a contact algorithm based on the penalty method was employed. The penalty method was implemented in the LS-DYNA software [12], with the fluid defined as the slave part and the tank structure as the master levels. Considering the two-dimensional nature of the modelling in this study, the node-to-solid method was used to evaluate the contact between the fluid and the structure [13]. The penetration of fluid particles into structural components was assessed using equation (1) [14].

$$l = \vec{n} \cdot (\vec{t} - \vec{r}) \tag{1}$$

where l is the penetration depth, $\vec{n}$ is the normal vector of the master element, $\vec{t}$ is the slave particle position vector and $\vec{r}$ is the contact point position vector. If the penetration depth is less than zero, SPH particles penetrate the slave part to the master element. As a result, the penalty force defined according to the following equation is activated [15]:

$$\vec{F}_p = (k_{cs} \times l)\,\vec{n} \tag{2}$$

In this equation, $\vec{n}$ indicates the vector that the normal of the master surface includes the contact point and k_{cs} represents contact stiffness. Due to the contact between dissimilar materials (fluid and tank), the soft constraint penalty formulation has been used to calculate the contact stiffness k_{cs}, which is determined based on the following relationship [16]:

$$k_{cs} = 0.5 \times SOFCL \times m \left(\frac{1}{\delta t_{cs}}\right)^2 \tag{3}$$

According to the above relationship, $SOFCL$ is the scale factor of the fixed soft constraint algorithm, m is a function of the mass of the node of the slave part and the master level, and δt_{cs} is the first time-step chosen to solve the problem. The fixed soft constraint algorithm enables a more nuanced treatment of constraints. It does not rigidly enforce boundaries, making it adaptable to real-world variability. On the other hand, the standard contact algorithm ensures strict adherence to constraints without compromise. By balancing constraint satisfaction with other objectives, the fixed soft constraint algorithm offers a more dynamic approach. The difference between the two soft constraint algorithms and the standard contact algorithm is that the first algorithm prevents abnormal and excessive penetration by creating secondary stiffness. The stiffness matrix in the fixed soft constraint algorithm is compared with the stiffness matrix in the standard contact algorithm, and the maximum is selected from the two. Using equation (3), the stiffness matrix is obtained in the standard contact algorithm [17]:

$$k_{cst} = f_s \frac{KA}{D} \tag{4}$$

where f_s is the scale factor, K is the bulk modulus, A is the contact surface and D is the maximum diameter. In order to prevent particle penetration, stabilize free surface flow, and mitigate fluid movement at high frequencies, artificial viscosity is incorporated. The tank model is depicted in Figure 2.

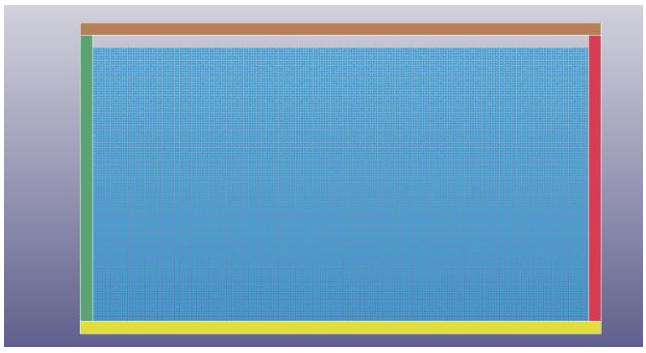

Fig. 2: Tank model.

3. Validation

When analysing the roof forces in concrete liquid storage tanks using numerical modelling, it is important to consider dynamic pressure. Dynamic pressure arises from the movement of stored liquid during seismic events or other disturbances. By using static equations, we can calculate this dynamic pressure, taking into account factors such as fluid

mass, acceleration, and tank geometry. Comparing the resulting dynamic pressure with the residual pressure (static pressure without considering fluid motion) allows us to verify the accuracy of our numerical model. For validating the model, concrete with the elastic modulus E_c, the density ρ_c, and the Poisson's ratio ν of 26.64GPa, $2400\ \frac{kg}{m^3}$ and 0.17 is considered respectively. Liquid is assumed to be water with material properties as mentioned in Table 1.

Table. 1: Material properties of water.

Parameter	ρ_0	v_d	C	γ_0	a	E_0	V_0
Value	1000 Kg/m^3	0.001 Pa.s	1448 m/s	0.11	3	0 J	0 m/s

where ρ_0, v_d, C, V_0, and E_0 are the initial density, the dynamic viscosity, the speed of sound in liquid, the initial relative volume of liquid, d, and the internal energy. Moreover, γ_0 is the Gruneisen gamma.

To validate the numerical modelling, a specific tank with dimensions outlined in Table 2 was chosen. Using LS-DYNA software [12], dynamic pressure at t=0.02s is calculated and depicted in Figure 3.

Table. 2: Tank characteristics.

Model Name	H_l (m)	H_w (m)	$2L_x$ (m)	$\frac{H_l}{2L_x}$	Fluid Particles Number
TS1	0.5	0.55	5	0.1	1000

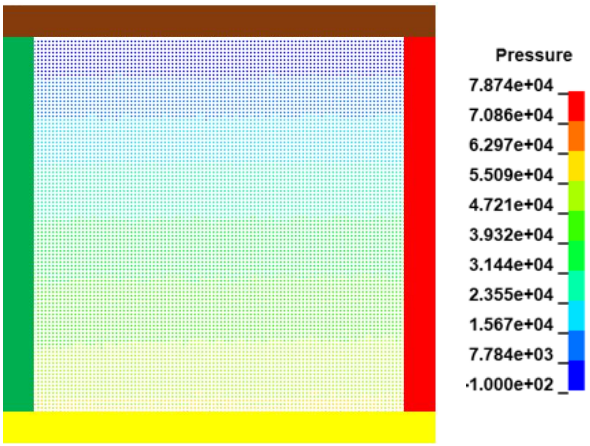

Fig. 3: Dynamic pressure in the tank.

Equation (5) establishes the static pressure within the TS1 model. Furthermore, the average dynamic pressure, illustrated as 5.11E04 in Figure 3, reinforces the model's reliability by highlighting the consistency between dynamic and static calculations.

$$P = \rho g h = 1000 * 9.807 * 20 = 4.903E + 04 \quad (5)$$

4. Numerical Studies

In this section, the impacts of geometric dimensions and frequency contents on the roof force will be examined. It is assumed in this study that the tank's roof, walls, and foundation are rigid, and soil-structure interactions are neglected. The responses are evaluated using the BBD method, with specific ranges chosen for tank length, ratio of liquid height to tank length, and seismic frequencies. The liquid storage tanks are exposed to the horizontal components of earthquakes from Northridge (1994), El-Centro (1940), Trinidad (1983), and Landers (1992), adjusted to achieve a peak ground acceleration of 0.4g. An analysis is conducted for the initial 20 seconds of each excitation, with time steps of 0.005s. In order to obtain reliable results, a mesh size and particle spacing of 5cm are utilized, and the tank's roof thickness is set at 50cm [9]. The characteristics of the earthquake records are detailed in Table 3.

Table 3: Seismic excitation properties [18].

Label	Year	station name	PGA(g)	PGV($\frac{m}{s}$)	$\frac{PGA}{PGV}$ ($\frac{1}{S}$)
Northridge	1994	Saticoy St	0.457	0.7484	0.61
El-Centro	1940	Array#9	0.319	0.3614	0.88
Landers	1992	Lucerne	0.782	0.3241	2.41
Trinidad	1983	CDMG ST1498	0.1936	0.1683	1.15

Tanks are categorized based on their size. When the length of the tank is 5m, it is considered small. The medium-sized tank has a length of 12.5m and the large-sized tank has a length of 20m. The second alphabet in each model represents its size category. Additionally, the height of the tank roof is set to be 5 centimetres higher than the height of the liquid it contains. Table 4 illustrates each model's geometric parameters.

Table 4: Geometric parameters of each model.

Model Name	H_l (m)	H_w (m)	$2L_x$ (m)	$\frac{H_l}{2L_x}$	Fluid Particles Number
TSP1	0.5	0.55	5	0.1	1000
TSP2	2.75	2.8	5	0.55	5500
TSP3	5	5.05	5	1	10000
TMP1	1.25	1.3	12.5	0.1	6250
TMP2	6.875	6.88	12.5	0.55	34375
TMP3	12.5	12.55	12.5	1	62500
TLP1	2	2.05	20	0.1	16000
TLP2	11	11.05	20	0.55	88000
TLP3	20	20.05	20	1	160000

where H_l, H_w, and $2L_x$ represent the height of the liquid, the height of the tank, and the tank length, respectively. Figure 4-8 depicts time history of roof force under defined seismic excitation and the results are summarised in Table 5. As mentioned earlier, the ratio of the fluid height to the length of the tank, the length of the tank and the earthquake record are some of the most important parameters in liquid storage tanks. As it is evident in Table 5, the force on the roof of the tanks increases with the reduction of the PGA/PGV and the increase of the fluid height in the structure. However, in several cases (such as rows: 2,3 and 17 in Table 5), the mentioned rule is violated. Therefore, it is not possible to have a detailed description of the effect of the selected parameters on the force on the roof of the tanks without statistical analysis. Nevertheless, it seems that other parameters should be checked for a more accurate evaluation of the force on the roof of the tanks.

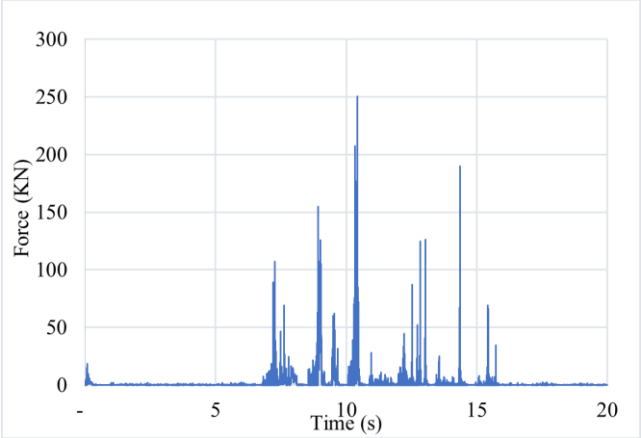

Fig. 4: Time history of roof force in TMP1 under landers earthquake.

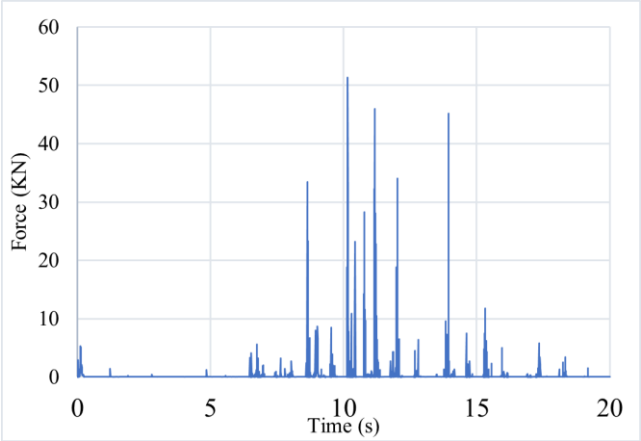

Fig. 5: Time history of roof force in TSP2 under landers earthquake.

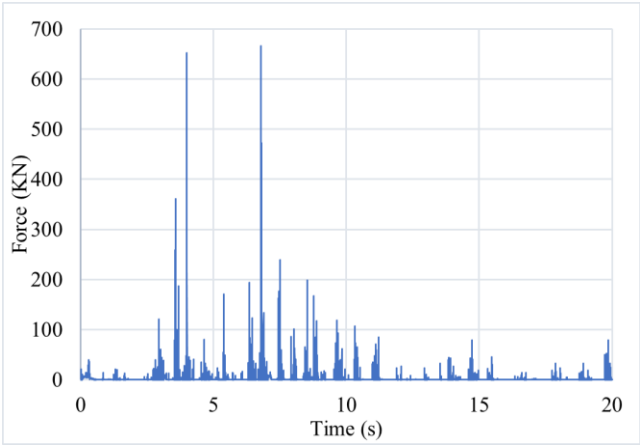

Fig. 6: Time history of roof force in TSP2 under Northridge earthquake.

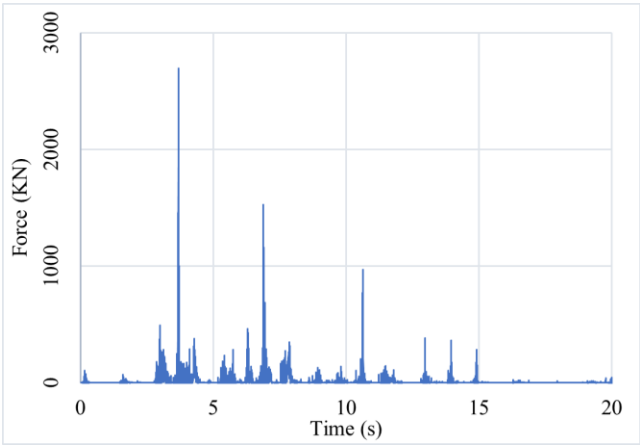

Fig. 7: Time history of roof force in TMP3 under Northridge earthquake.

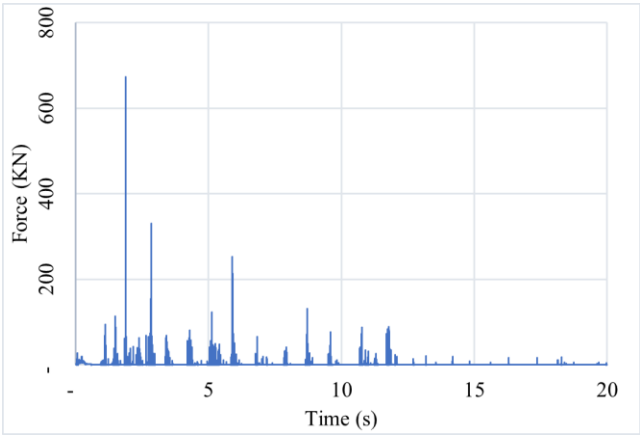

Fig. 8: Time history of roof force in TSP3 under EL-Centro earthquake.

Table 5: Geometric parameters of each model.

Earthquake	No.	Model Name	$2L_x$ (m)	H_l (m)	Roof Force *(KN)*
Landers	1	TMP1	12.5	1.25	250
	2	TMP3	12.5	12.5	169
	3	TLP2	20	11	663
	4	TSP2	5	2.75	51
Northridge	5	TMP3	12.5	12.5	2697
	6	TMP1	12.5	1.25	2211
	7	TLP2	20	11	8300
	8	TSP2	5	2.75	666
EL-Centro	9	TLP3	20	20	1525
	10	TLP1	20	2	2917
	11	TMP2	12.5	6.875	1422
	12	TSP3	5	5	674
	13	TSP1	5	0.5	683
Trinidad	14	TMP1	12.5	1.25	884
	15	TMP3	12.5	12.5	1580
	16	TLP2	20	11	763
	17	TSP2	5	2.75	557

Table 6 illustrates a Comparison of roof force under El-Centro earthquake for different models. For roofed tanks under the same horizontal excitation, for two tanks with equal length, if the ratio of the height of the fluid to the length of the tank increases, the maximum force on the roof of the tank increases. Also, for two tanks with the same ratio of fluid height to tank length, as illustrated in Figure 9 and Figure 10, increasing the tank length increases the force on the tank roof, and the effect of the tank length parameter is greater than the fluid height.

Table 6: Comparison of roof force under El-Centro earthquake.

Earthquake	Model Name	$2L_x$ (m)	H_l (m)	$\frac{H_l}{2L_x}$	Roof Force (KN)
EL-Centro	TLP3	20	20	1	1525
	TLP1	20	2	0.1	2917
	TMP2	12.5	6.875	0.55	1422
	TSP3	5	5	1	674
	TSP1	5	0.5	0.1	683

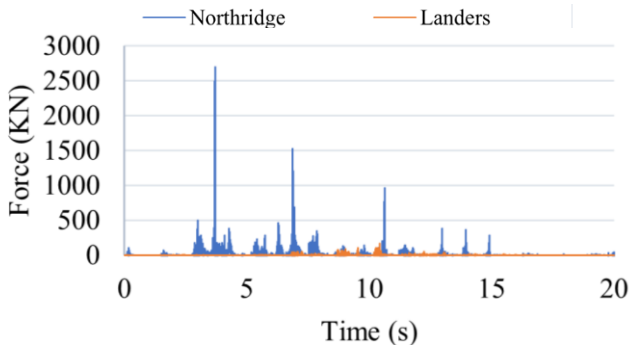

Fig. 9: Time history of roof force in TMP3.

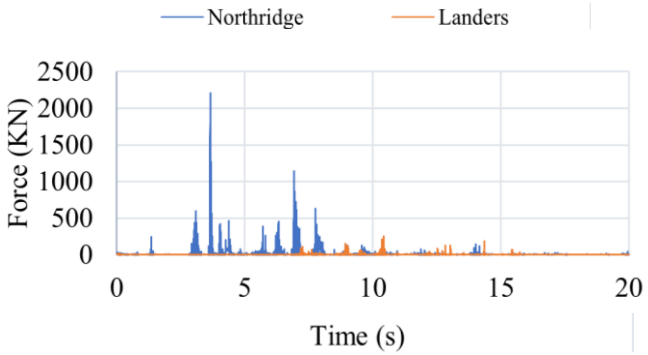

Fig. 10: Time history of roof force in TMP1.

The acceleration spectrum intensity (ASI) was originally proposed as a valuable metric for seismic analysis of concrete dams based on the natural vibration characteristics of the liquid in the tanks. Thun et al. [19] defined ASI as the integral of the pseudo-spectral acceleration over a period range from 0.1s to 0.5s. The mathematical representation for ASI is provided by [19].

$$ASI = \int_{0.1}^{0.5} S_a(T, 5\%)dT \quad (6)$$

where Sa(T,5%) is the 5% damped spectral acceleration at a specific vibration period T. Table 7 compares each earthquake record's ASI.

As mentioned above, the BBD method was implemented, therefore, two different designs were conducted. Table 8 demonstrates the parametric ranges in these two designs.

In the first design three parameters $\frac{H_l}{2L_x}$, $2L_x$, and PGA/PGV of Trinidad, El-Centro and Northridge are selected. The analysis results are given in Figures 11 and 12. Figure 11 shows the effect of each parameter of roof force, and Figure 12 depicts the Pareto chart of the standardized effects. As for the second design, three parameters $\frac{H_l}{2L_x}$, $2L_x$, and PGA/PGV of Trinidad, El-Centro and Northridge are selected. The analysis results are given in Figures 13 and 14. Figure 13 shows the effect of each parameter on roof force, and Figure 14 depicts the Pareto chart of the standardized effects.

Table 7: ASI of earthquake records.

Record	ASI (g x sec)
Northridge	0.442
EL-Centro	0.394
Landers	0.185
Trinidad	0.344

Table 8: parameters range in each design.

DOE num.	Parameters	Min	Mid	Max
1	PGA/PGV	0.61	0.88	1.15
	$2L_x$	5	12.5	20
	$\frac{H_l}{2L_x}$	0.1	0.55	1
	ASI	0.344	0.394	0.442
2	$2L_x$	5	12.5	20
	$\frac{H_l}{2L_x}$	0.1	0.55	1

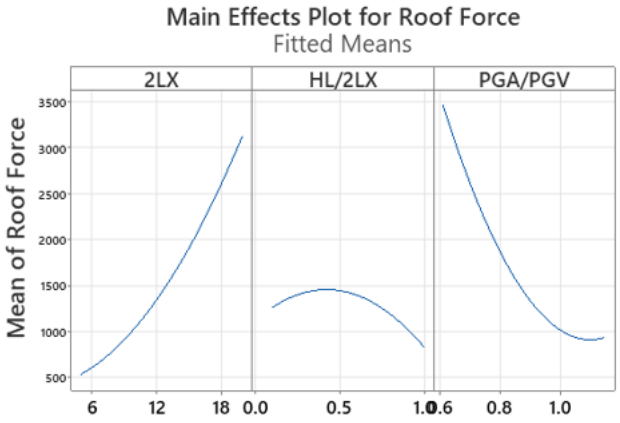

Fig. 11: main parameters effects in the first design.

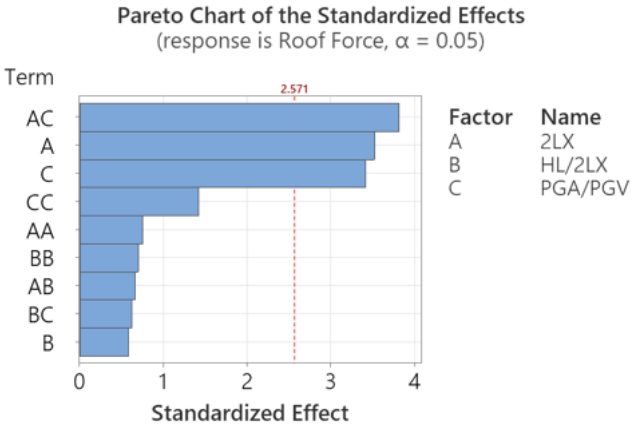

Fig. 12: Pareto chart of the standardized effects in the first design.

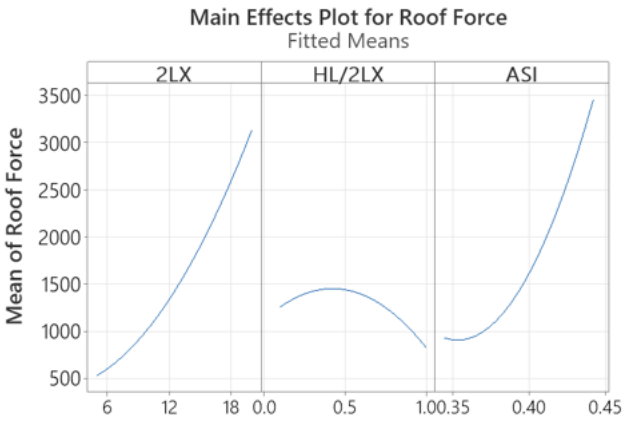

Fig. 13: main parameters effects in the second design.

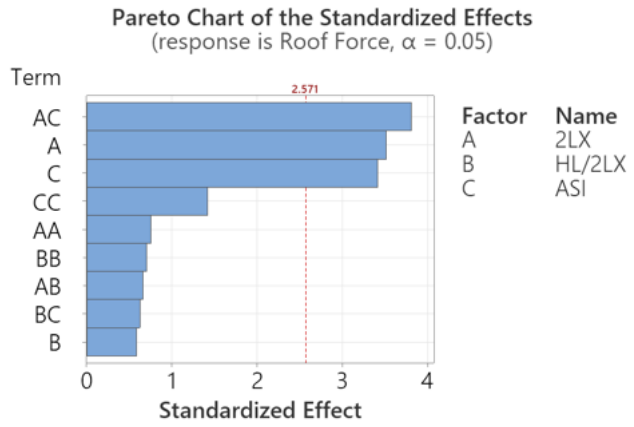

Fig. 14: Pareto chart of the standardized effects in the second design.

As can be seen, in the first design:

- The most influential parameter on the force on the tank roof is the combination of two parameters $2L_x$ and PGA/PGV.
- Increasing the $2L_x$ increases the force on the roof, and decreasing the PGA/PGV ratio causes a decrease in the force on the roof of the tanks.
- The effect of the parameter $\frac{H_l}{2L_x}$ is insignificant and therefore it can be concluded that the parameter H_l is noise.
- Using the BBD method roof force in concrete liquid storage tanks can be estimated with equation (7).

$$\begin{aligned} Roof\ Force\ (KN) = & -421 + 913(2L_X) + 5226\left(\frac{H_l}{2L_X}\right) \\ & - 9534\left(\frac{PGA}{PGV}\right) + 7.26(2L_X * 2L_X) \\ & - 1880\left(\frac{H_l}{2L_X} * \frac{H_l}{2L_X}\right) \\ & + 10581\left(\frac{PGA}{PGV} * \frac{PGA}{PGV}\right) \\ & - 102\left(\frac{H_l}{2L_X} * 2L_X\right) - 983\left(2L_X * \frac{PGA}{PGV}\right) \\ & - 2681(\frac{H_l}{2L_X} * \frac{PGA}{PGV}) \end{aligned} \quad (7)$$

As for the second design:

- The most influential parameter on the force on the tank roof is the combination of two parameters ASI and $2L_x$.
- Increasing the parameter $2L_x$ increases the force on the ceiling and the effect of the parameter $\frac{H_l}{2L_x}$ is insignificant. Thus, it can be concluded that the parameter H_l is noise.
- by using this method, it is possible to calculate the maximum force on the roof using the following equation (8):

$$\begin{aligned} Roof\ Force\ (KN) = & 68685 - 2080(2L_X) - 2939\left(\frac{H_l}{2L_X}\right) \\ & - 302601(ASI) + 7.26(2L_X * 2L_X) \\ & - 1880\left(\frac{H_l}{2L_X} * \frac{H_l}{2L_X}\right) \\ & + 321272(ASI * ASI) - 102\left(\frac{H_l}{2L_X} * 2L_X\right) \\ & + 5416(2L_X * ASI) + 14773(\frac{H_l}{2L_X} * ASI) \end{aligned} \quad (8)$$

The formulations presented in this section enable the estimation of roof forces in tanks characterized by both geometric and seismic properties range outlined in Table 7. Notably, the maximum error associated with these estimates remains within a 20% margin. Ultimately, it can be said that the PGV/PGA ratio has an opposite behavior with respect to ASI when dealing with roof force in liquid storage tanks.

5. Conclusion

Extensive studies have been conducted in the field of dynamic response of fluid storage tanks, despite these studies, many issues in this field remain unanswered. This study has evaluated 51 models of tanks with different characteristics to investigate the nonlinear dynamic response of two-dimensional tanks. In this way, goals such as determining the effect of geometric and seismic parameters on the force on the roof have been pursued. Although the FE-SPH method increased computational costs, it demonstrates promising results in capturing complex behavior of the fluid. In contrast, the Box-Behnken DOE method significantly reduces time and resource requirements by employing fewer experimental analysis than full factorial designs.

In general, according to the results and evaluations shown in this article and in Soltani et al. 2024 [9], The behavior of tanks without free height and with free height is different. it can be said that the most important factor in the design of concrete tanks is the frequency content. Also, by comparing the statistical results, it is clear that the behavior of the sloshing height and the force on the roof are not the same. This is important because in the evaluation of the maximum sloshing height, the length of the tank is noise and in the evaluation of the force acting on the ceiling of the tank, fluid height is a noise parameter. Also, the length of the tank is the most important geometric parameter in the investigation of the pressure on the roof of the tanks, and fluid height is the most crucial parameter in the sloshing height. Regarding the seismic records used in Benken box designs, it can be concluded that PGA/PGV and ASI can be suitable parameters to calculate responses. However, it is clear from the graphs of this article that ASI is a more suitable parameter in evaluating the behavior of a tank.

Two formulations proposed in this study can calculate the force on the roof of the tanks. these formulations can only be used for tanks whose design parameters (tank length, fluid height, and seismic excitation) are within the indicated range.

References

[1] Malhotra PK, "Earthquake induced sloshing in tanks with insufficient freeboard. " Structural Engineering International,vol.16., 2006,222–225

[2] Malhotra, P. K. "Sloshing loads in liquid-storage tanks with insufficient freeboard", Earth quake Spectra ,vol.21 (4), 2005,1185–1192.

[3] Yoshida, Shoichi, Kazuyoshi Sekine, and Tsukasa Mitsuta. "Axisymmetric finite element analysis for sloshing response of floating roofs in cylindrical storage tanks." Journal of Environment and Engineering 5, no. 1 (2010): 27-38.

[4] Golzar, F. G., R. Shabani, S. Tariverdilo, and G. Rezazadeh. "Sloshing response of floating roofed liquid storage tanks subjected to earthquakes of different types." (2012): 051801.

[5] Livaoglu R, Turan A, El Naggar MH, Dogangun A. The numerical and empirical evaluation of structural performance of elevated tanks considering soil–structure interaction effects. Journal of Earthquake and Tsunami. 2012 Jun;6(02):1250008.

[6] Goudarzi, Mohammad Ali. "Seismic design of a double deck floating roof type used for liquid storage tanks." Journal of Pressure Vessel Technology 137, no. 4 (2015): 041302.

[7] Hosseini, Mahmood, Mohammad Ali Goudarzi, and Amirhossein Soroor. "Reduction of seismic sloshing in floating roof liquid storage tanks by using a Suspended Annular Baffle (SAB)." Journal of Fluids and Structures 71 (2017): 40-55.

[8] Nouraeidanesh, P., M. M. Kabiri, and M. A. Goudarzi. "An innovative roof shape in liquid storage tanks to reduce dynamic sloshing effects." Journal of Applied Fluid Mechanics 11, no. 1 (2018): 127-136.

[9] Soltani, Pouya, and Hassan Mirzabozorg. "Parametric analysis of sloshing in concrete liquid storage tanks: a FE-SPH coupled approach with Box-Behnken design of experiments." Journal of the Brazilian Society of Mechanical Sciences and Engineering 46, no. 6 (2024): 1-24.

[10] Ferreira, SL Costa, R. E. Bruns, Hadla Sousa Ferreira, Geraldo Domingues Matos, J. M. David, G. C. Brandão, EG Paranhos da Silva et al. "Box-Behnken design: An alternative for the optimization of analytical methods." Analytica chimica acta 597, no. 2 (2007): 179-186.

[11] de Castro Peixoto, André Luís, Ademir Geraldo Cavallari Costalonga, Mateus Nordi Esperança, and Rodrigo Fernando dos Santos Salazar. "Design of experiments applied to antibiotics degradation by Fenton's reagent." Statistical Approaches With Emphasis on Design of Experiments Applied to Chemical Processes (2017).

[12] LSTC Inc. LS-DYNA software V.971 R11.0. (2018).

[13] LS-DYNA keyword user's manual: nonlinear dynamic analysis of structures. Version 971, vols 1 and 2. Livermore Software Technology Corporation; October 2018.

[14] Lee, Sangmin, and Jung-Wuk Hong. "A Semi-Infinite Numerical Wave Tank Using Discrete Particle Simulations." Journal of Marine Science and Engineering 8.3 (2020): 159.

[15] Liu, Xiaohui, Songyong Liu, and Huifu Ji. "Numerical research on rock breaking performance of water jet based on SPH." Powder Technology 286 (2015): 181-192.

[16] Lee, Sangmin, and Jung-Wuk Hong. "Parametric studies on smoothed particle hydrodynamic simulations for accurate estimation of open surface flow force." International Journal of Naval Architecture and Ocean Engineering 12 (2020): 85-101.

[17] Pham, Thong M., Yifei Hao, and Hong Hao. "Sensitivity of impact behaviour of RC beams to contact stiffness." International Journal of Impact Engineering 112 (2018): 155-164.

[18] Pacific Earthquake Engineering Research Center (2005) PEER Strong Motion Database on Line. Berkley. https://peer.berkeley.edu/peer-strong-ground-motion-databases.

[19] Von Thun, J. Lawrence. "Earthquake ground motions for design and analysis of dams." Earthquake engineering and soil dynamics II-recent advances in ground-motion evaluation (1988).